JOURNAL OF
Optical Communications
and Networking

Large-scale and nonblocking OXC using a hybrid of WSSs and OCSs

Dannan Hong,[1,†] Tong Ye,[1,*,†] Qiang Guo,[2] Bofang Zheng,[2] Zhiwu Chang,[2] Ruishan Chen,[2] and Luo Han[2]

[1]State Key Laboratory of Photonics and Communications, Shanghai Jiao Tong University, Shanghai, China
[2]Huawei Technologies Co., Ltd., Shenzhen, China
[†]These authors are co-first authors.
*yetong@sjtu.edu.cn

Received 29 April 2025; revised 19 June 2025; accepted 12 July 2025; published 19 August 2025

The surge in Internet traffic is driving traditional single-fiber fixed-grid optical networks to change toward multi-fiber flex-grid networks with fewer wavelengths per fiber. Designing a large-scale optical cross-connect (OXC) to adapt to these changes is challenging because the scalability of standard OXCs is limited by the port count of the wavelength-selective switch (WSS). The existing proposals either suffer from high insertion loss, lack a non-blocking property, or cannot support flexible grids. To this end, we propose a class of heterogeneous OXCs, using WSSs and port-level optical circuit switches (OCSs). Our idea is to employ WSSs to handle wavelength switching and OCSs to scale up the dimension of the OXC. In the context of flexible grids, we prove the conditions under which the heterogeneous OXCs are nonblocking on the line side, and colorless, directionless, and contentionless on the add/drop side. Also, our analysis shows that the port count of WSSs required by our proposals is governed only by the number of wavelengths in the network, rather than the dimension of the OXC. Also, our designs have low loss and a small filtering effect, as each lightpath only needs to pass through up to two WSSs in the OXC.

https://doi.org/10.1364/JOCN.566633

1. INTRODUCTION

Driven by the explosive growth of Internet traffic, optical transport networks (OTNs) are undergoing a new round of capacity expansion and exhibiting three development trends. First, installing multiple fibers or multi-core fibers in each optical link, known as spatial division multiplexing (SDM), has been considered an efficient way to enhance link capacity [1]. Second, the channel spacing of wavelength division multiplexing (WDM) systems will climb from 50 GHz to 300 GHz [2,3]. As a result, the number of wavelength channels in the C+L band will decline to 40 in the next few years. Third, traditional fixed-grid optical networks will be replaced by flex-grid networks, which should be able to support lightpaths of different bandwidths.

As a core component of optical nodes, the optical cross-connect (OXC) should be redesigned to cope with the changes of the OTN. As Fig. 1 depicts, a standard OXC is a wavelength-selective switch (WSS) based full-mesh switching fabric, which can not only perform nonblocking switching but also support flexible grids [4–7]. However, the scalability of a standard OXC is limited by WSSs. As Fig. 1 shows, the port count of a standard OXC is determined by that of WSSs. The port count of current commercial WSSs is 49, and it is hard to increase due to the difficulty in the control of insertion loss and crosstalk [8]. As a result, only 48 port standard OXCs can be manufactured by now [9]. However, the number of fibers on each link will be massive in the future [1], implying that the port count of OXCs will be large. Hence, designing a scalable OXC is an urgent yet challenging task.

From the perspective of industrial application, a large-scale OXC would be better to possess seven features as follows.

P1: it is scalable such that the port count of the WSS required by the OXC can be small when compared to the port count of the OXC.

P2: it can support flexible grids.

P3: it is not reliant on optical components (e.g., wavelength converters (WCs)) that may not be commercialized in the near future.

P4: its insertion loss can be as low as possible.

P5: it can inherit the nonblocking property of the standard OXC, thereby eliminating the need to consider the internal switching state of OXCs when performing routing and spectrum assignment (RSA) [10] in the optical network.

P6: it should have a pay-as-you-grow (PAYG) property [11].

P7: the number of optical components cannot be very large.

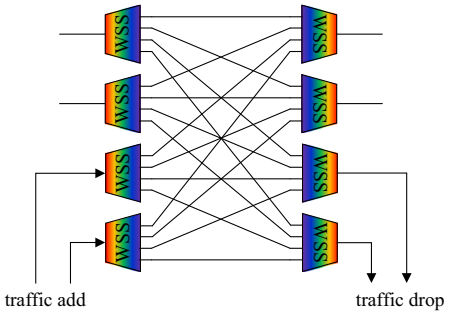

Fig. 1. The dimension of the standard OXC is completely determined by the port count of the WSSs.

A. Previous Works

Up to now, a lot of effort has been dedicated to the design of scalable OXCs, which are either nonblocking or blocking.

A type of nonblocking OXC was designed based on an arrayed waveguide grating (AWG) and an optical circuit switch (OCS) [12,13], which is a wavelength-insensitive port-level optical switching device. An $N \times N$ AWG-based OXC includes $2N$ $1 \times W$ AWGs on both sides and W $N \times N$ OCSs in the center, where N is the port count of the OXC and W is the number of wavelengths on each fiber. The AWG-based OXC has ∼14 dB insertion loss on the line side. Also, it can be expanded to a large scale because the port count of the current commercial OCS is 512 [14]. The major drawback of the AWG-based OXC is that it does not support flexible grids since the AWG is a fixed-grid optical device.

The nonblocking scalable OXCs in [15–18] are designed based on the theory of Clos networks [19]. We call this kind of OXC the OXC-Clos network, where each switching module is a small-scale standard OXC. In particular, Ref. [15] studies the ability of the OXC-Clos network with and without WCs to build up a lightpath from an input to an output if there are idle transceivers at the input and the output. However, this paper does not consider flexible grids when performing the design. Reference [18] further studies the nonblocking conditions of flex-grid OXC-Clos networks without WCs. The OXC-Clos network has the following drawbacks: (a) it requires a remarkable additional cost to support flexible grids, as Ref. [18] proves, and (b) each lightpath suffers from a high insertion loss because it has to traverse three standard OXCs.

Reference [20] proposes a three-phase modularization approach for transforming a standard OXC into a modular OXC while preserving its nonblocking property. This structure enables the design of large-scale OXCs using small-scale WSSs and OXC modules. However, the number of small-scale OXCs in this design increases linearly with the port count of the module OXC.

References [21–23] provide another choice to construct modular OXCs, called space-wavelength-space (SWS) and wavelength-space-wavelength (WSW) switches. These two OXC architectures are designed to support flexible grids. However, they need bandwidth-variable wavelength-converting switches (BV-WSs), which are far from being commercialized.

An early design of large-scale internally blocking OXCs is the hierarchical optical path cross-connect (HOXC) [11,24–29], which is motivated by the argument as follows. In future OTNs, the majority of lightpaths will merely necessitate fiber-level switching, and only a minority will require wavelength-level switching. The HOXC consists of an OCS and a standard OXC. In particular, the OCS connects with the OXC via a small portion of its input/output ports. Let h be this portion. If all the lightpaths on an input fiber head for the same output fiber, they will be switched together by the OCS; otherwise, they are fed by the OCS to the OXC for wavelength-level switching. The HOXC with $h < 1$ is blocking, meaning that the HOXC reduces the port count of the WSS at the expense of the nonblocking property. The HOXC has the following two issues. On the one hand, the port count of the WSS still linearly increases with the dimension of the HOXC. On the other hand, it is difficult to adjust h according to the traffic demand in the future, after the HOXC is deployed.

References [30–34] devise a ring-type large-scale OXC network by interconnecting multiple small-scale standard OXC modules. In this design, the lightpaths may suffer different insertion losses as they may traverse different numbers of small-size OXCs inside the OXC network. The loss could be large if a lightpath needs to pass through several small-sized OXCs.

References [35–37] propose a heterogeneous large-scale OXC, called HIER. The idea is to replace each $1 \times N$ WSS in a standard OXC by a $1 \times k$ WSS cascaded by k $1 \times m$ wavelength-insensitive optical space switches, where $km = N$. Though the replacement reduces the requirement on the dimension of WSSs, it weakens the flexibility of the OXC. Hence, Ref. [10] has to develop a complicated RSA algorithm for the network equipped with such a kind of OXC, to minimize the blocking probability of lightpath requests.

References [38,39] improve the scalability of OXCs by reducing the number of interconnection links between the WSSs at the input and output sides. Specifically, the WSSs on the input side only connect with a small number of the WSSs on the output side and vice versa. The idea behind this design is to make use of the difference between nodal degree and fiber degree. A lightpath can reach its desired destination, as long as it can be switched to one of the fibers in a nodal degree. However, this type of OXCs is also blocking.

Though Ref. [40] demonstrates that a well-designed RWA algorithm can alleviate the negative impact of internal blocking of OXCs on the network-level blocking probability. The time complexity will be very high, e.g., $O(V^4 + WV^2)$ in [40], where V is the number of optical nodes and W is the number of wavelengths.

In summary, none of the previous designs possesses all the properties P1 to P7 at the same time. This motivates our work in this paper.

B. Our Works

In this paper, we propose a family of heterogeneous OXCs by combining the merits of WSSs and OCSs. Our goal is to design an OXC that possesses properties P1 to P7 at the same time for near-future application scenarios, where there are a large number of fibers per link and a small number of wavelengths per fiber. Herein, the "link" stands for a fiber duct between two optical nodes.

The heterogeneous OXCs are based on the complementary features of WSSs and OCSs. The WSS excels at wavelength switching but falls short in port count and loss. In contrast, the OCS, despite its wavelength insensitivity, boasts scalability and a low loss profile. We thus propose our design principle: the WSS handles wavelength switching, while the OCS caters to dimension expansion.

Under this principle, we propose three-stage heterogeneous OXC architectures. The input/output stage consists of a column of WSSs and a set of OCSs. At the input/output stage, each WSS is deployed as an ingress/egress module on the line side, and each OCS is used as an add (or drop) module and is connected to a transceiver (or receiver). The central stage is an OCS-based switching network. Following this framework, we devise three OXC structures, named Clos-type OXC, Butterfly OXC, and expandable Butterfly OXC.

After analyzing the routing constraints in three proposed OXCs, we derive nonblocking conditions on the line side and colorless-directionless-contentionless (CDC) conditions on the add/drop (A/D) side, in the flex-grid context. Our analytical results show that the port count of WSSs required by our proposals is determined solely by the number of wavelengths, instead of the dimension of the OXC. This confirms that these three designs are suitable for future application scenarios.

Moreover, we find that the port count of WSSs required by the Butterfly OXC and expandable Butterfly OXC exactly equals the wavelength count, roughly half of that in the Clos-type OXC, meaning that the Butterfly OXC and expandable Butterfly OXC are more scalable than the Clos-type OXC. On the other hand, the Clos-type OXC has less insertion loss on the A/D side than the Butterfly OXC and expandable Butterfly OXC.

The remainder of this paper is organized as follows. Section 2 first briefly introduces the functions of WSSs and OCSs and then presents the principle, assumption, and overview of our design. Sections 3 and 4 propose the Clos-type OXC, Butterfly OXC, and expandable Butterfly OXC and derive the nonblocking and CDC conditions, respectively. Section 5 compares three proposed OXCs and previous architectures. Section 6 concludes this paper.

2. PRELIMINARY

To facilitate the presentation, we first introduce the functions of WSSs and OCSs, which are the building blocks of our designs, in Section 2.A. From this introduction, we come up with the design principle of our heterogeneous OXC structures. In Section 2.B, we then present our assumption adopted in this paper. After that, we provide an overview of our proposal, as well as relevant terminologies and definitions in Section 2.C.

A. Principle of Our Design

Our designs are inspired by the complementary features of WSSs and OCSs, which are briefly introduced as follows.

The WSS is a wavelength-sensitive optical component. A $1 \times k$ WSS can switch each wavelength from the input to any of the outputs, independent of other wavelengths. Figure 2(a) illustrates an example of a 1×2 WSS, which switches red and blue wavelengths to output 1 while switching green and yellow ones to output 2.

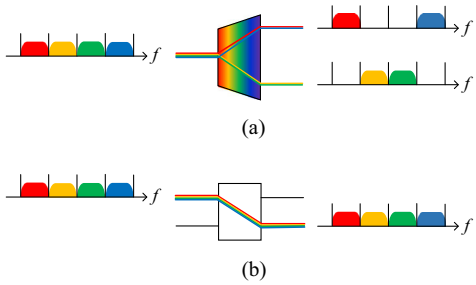

Fig. 2. Two types of building blocks, where each slot represents a wavelength channel and each solid box represents the spectrum occupied by a lightpath: (a) 1×2 WSS and (b) 2×2 OCS.

Though the WSS is a flexible switching fabric, it has two drawbacks. First, the increase of port count is not easy due to the difficulty in the control of crosstalk and insertion loss in the manufacturing process. As Section 1 mentions, the dimension of the OXC will increase very rapidly due to the deployment of the SDM technique. This implies that the port limitation of WSSs hinders the prompt scaling-up needs of the OXC. Second, its insertion loss is 6 dB [41]. This makes the classical theory of multi-stage switching networks not applicable to the expansion of OXCs, unless some techniques can be developed to lower the insertion loss.

The OCS is a port-level optical switch and cannot separate different wavelengths and switch them to different outputs. That is, the OCS can only switch all the wavelengths in a fiber as a whole from its input to its output, as Fig. 2(b) plots. However, the OCS has a low insertion loss, and its port count can be easily increased. The current commercial OCS, such as a micro-electromechanical system (MEMS)-based OCS [42] and a Piezo-actuator-based OCS [43], typically exhibits an insertion loss of 2 dB and can support a reach of 512.

Obviously, the WSS and the OCS have complementary features, from which we propose the following design principle:

Design Principle: the WSS copes with the wavelength switching, while the OCS caters to the dimension expansion of the OXC.

We will show that this principle ensures that the port count of the WSS will not increase with the dimension of the OXC.

B. Assumption of Our Work

Our scalable OXCs will be designed based on the following assumption:

Assumption: *the number of fibers per link will be large, while the number of wavelengths per fiber is small*.

This assumption stems from the development trends of OTNs. On one hand, the number of fibers per link is increasing rapidly, as we present in Section 1. On the other hand, a 150-GHz channel-spacing transmission system has already been commercialized [44], and 200-GHz and 300-GHz channel-spacing systems will become commercially available in the next five or 10 years. Consequently, the number of wavelength channels in the 12 THz C+L band will decline from 80 to 60 or 40 in the coming years.

C. Overview of the Proposed OXCs

Figure 3 displays the general structure of our proposed OXCs, where there are r input WSSs (IWs) and r output WSSs (OWs) on the line side, and r' add OCS modules (AMs) and r' drop OCS modules (DMs) on the A/D side. The part in the dotted box is an OCS-based switching network. Different designs of this part yield various derived proposals, as we will show in Sections 3 and 4.

The IWs and the OWs are connected with other optical nodes in the network. We number the IWs by $1, \ldots, \alpha, \ldots, r$, and the OWs by $1, \ldots, \beta, \ldots, r$. Each IW and each OW carry W wavelength channels in the C+L band. We label these W wavelengths by $1, \ldots, w, \ldots, W$.

Each AM contains n inputs, each of which is attached by a transmitter (Tx), and each DM has n outputs, each of which is linked to a receiver (Rx). The AM and DM are connected with local electrical switches via Txs and Rxs, respectively. A Tx can only launch one lightpath, and an Rx can only terminate one lightpath. We number the AMs by $1, \ldots, \alpha', \ldots, r'$ and the DMs by $1, \ldots, \beta', \ldots, r'$.

The OXC needs to carry three types of lightpaths and can generate two types of lightpath requests. A lightpath (request) from an IW to an OW is called a bypass lightpath (request), that from an add port to an OW is called an add lightpath (request), and that from an IW to a DM is called a drop lightpath. A lightpath (request) in the flex-grid optical network can employ ω adjacent wavelengths, where $1 \le \omega \le W$. This paper refers to a lightpath (request) using ω wavelengths as a ω-granularity (ω-g) lightpath (request). Note that the OXC never generates a lightpath from an add port to a drop port.

Let $\mathbf{\Lambda}_w^\omega$ be a collection of ω adjacent wavelengths that starts from wavelength w and ends at wavelength $w+\omega-1$, where $w \ge 1$ and $w+\omega-1 \le W$. We denote a bypass request as $R_{\text{bp}}(\alpha, \beta, \mathbf{\Lambda}_w^\omega)$, if it uses a wavelength set $\mathbf{\Lambda}_w^\omega$, and originates from IW α and heads for OW β. Figure 3 illustrates a request $R_{\text{bp}}(1, r, \mathbf{\Lambda}_w^\omega)$, which arises from IW $\alpha = 1$ and ends at OW $\beta = r$, and uses wavelength set $\mathbf{\Lambda}_w^\omega$. We say R_{bp} is legal if all the wavelengths in $\mathbf{\Lambda}_w^\omega$ are free on both IW α and OW β. We denote an add request as $R_{\text{add}}(\alpha', a, \beta, \mathbf{\Lambda}_w^\omega)$, if it uses a wavelength set $\mathbf{\Lambda}_w^\omega$, and originates from input a of AM α' and heads for OW β. We say R_{add} is legal if all the wavelengths in $\mathbf{\Lambda}_w^\omega$ are free on OW β and input a of AM α' stays idle.

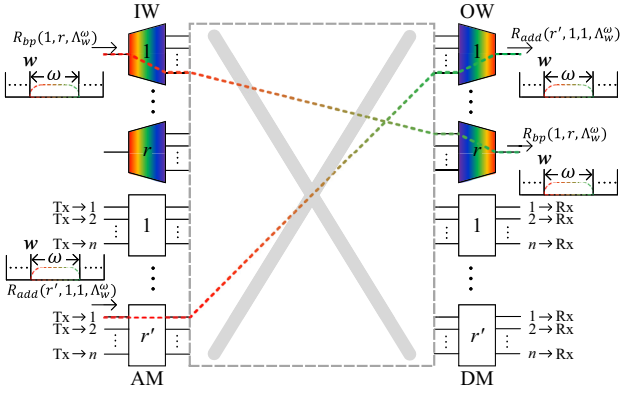

Fig. 3. Overview of our proposed OXC, where each colorful hollow dotted box represents the spectrum required by a lightpath request.

$R_{\text{add}}(r', 1, 1, \mathbf{\Lambda}_w^\omega)$ in Fig. 3 is an example. In a similar way, we denote a legal drop request from IW α to output b of DM β' as $R_{\text{drop}}(\alpha, \beta', b, \mathbf{\Lambda}_w^\omega)$.

This paper pursues the design of an OXC, which is nonblocking on the line side and CDC on the A/D side, such that the RSA in the optical network can be largely simplified. The nonblocking and CDC properties are defined as follows.

Definition 1: *an OXC is wide-sense nonblocking (WSNB) on the line side, if a routing strategy exists for setting lightpaths in such a way that a lightpath demanding a set of adjacent wavelengths can always be set up from an input port to an output port without rearranging the paths of the existing lightpaths when the wavelength set is free on the input port and the output port.*

Definition 2: *the OXC is CDC on the add side if an add port can always add any set of adjacent wavelengths to any output port without rearranging the paths of the existing lightpaths, as long as the add port has free Txs and the wavelength set is free on the output port.*

Definition 3: *the OXC is CDC on the drop side if a drop port can drop any set of adjacent wavelengths from any input port without rearranging the paths of the existing lightpaths, as long as the drop port has free Rxs.*

3. CLOS-TYPE OXC ARCHITECTURE

Figure 4 depicts the proposed Clos-type OXC, which is a three-stage network. Apart from the IWs, OWs, AMs, and DMs, the part in the dotted box in Fig. 3 is implemented by a column of m $(r+r') \times (r+r')$ central OCS modules (CMs) in the middle, which are numbered by $1, \ldots, \gamma, \ldots, m$.

In this network, two optical modules at adjacent stages are interconnected by exactly one fiber. Particularly, output γ of IW α is connected to input α of CM γ and output γ of AM α' is connected to input $r+\alpha'$ of CM γ. Also, output β of CM γ is linked to input γ of OW β and output $r+\beta'$ of CM γ is linked to input γ of DM β'. It follows that each IW and AM has m outputs, and each OW and DM has m inputs.

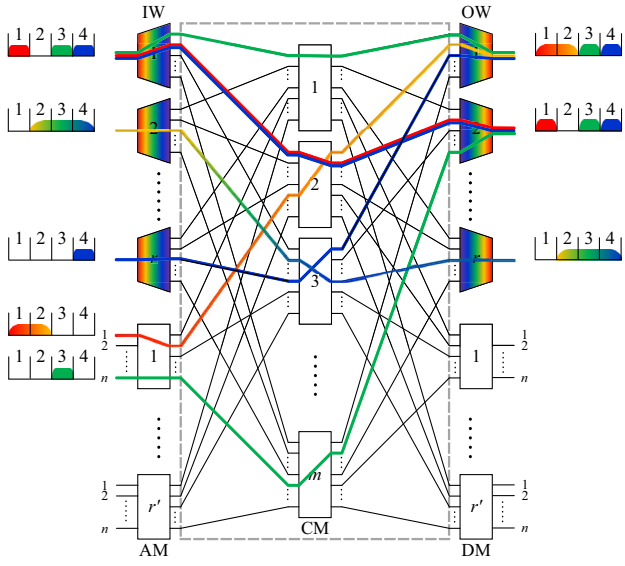

Fig. 4. Illustration of the Clos-type OXC.

A. Routing Constraints and CM-Sharing Routing

Wavelength insensitivity of OCSs imposes the following routing constraints:

C1: the lightpaths from the same IW to different OWs/DMs cannot share the same CM;
C2: the lightpaths from different IWs/AMs to the same OW cannot share the same CM;
C3: the lightpaths from the same AM or to the same DM cannot share the same CM.

These three constraints are illustrated in Fig. 4. The lightpaths from IW 1 to OW 1 and the one from IW 1 to OW 2 are not able to use the same CM. Similarly, the lightpath from IW 1 to OW 1 and that from IW r to OW 1 cannot share the same CM. Also, two lightpaths that both originate from AM 1 do not traverse the same CM.

On the contrary, two lightpaths can share the same CM, if

S1: they are all from the same IW to the same OW;
S2: they are from different IWs or AMs to different OWs or DMs.

As Fig. 4 illustrates that the two lightpaths from IW 1 to OW 2 can utilize the same CM, and both of them can share the same CM with the lightpath from AM 1 to OW 1. According to S1, we have the following routing strategy.

CM-Sharing Routing: all the lightpaths from the same IW to the same OW should use the same CM to minimize the usage of CMs as much as possible.

B. Nonblocking and CDC Conditions

Due to the routing constraints and the CM-sharing routing, we have to consider the following two scenarios separately when studying the nonblocking condition on the line side and the CDC condition on the A/D side.

The first scenario is identified by $W \le r + r'n$, where the number of CMs used by the lightpaths coming from an IW (or heading for an OW) that could reach W. An IW may launch up to W 1-g lightpaths that visit different OWs and different output ports of DMs. According to constraints C1 and C3, these W lightpaths will employ W CMs. Similarly, an OW might be accessed by up to W 1-g lightpaths that come from different IWs and different input ports of AMs. Figure 5(a) plots an example of this case, where $W = 4$, $r = 3$, $r' = 1$, and $n = 2$. IW 1 launches $W = 4$ 1-g lightpaths, which visit all $r = 3$ OWs and DM 1, respectively. Thus, they have to use $W = 4$ CMs, i.e., CMs 1, 2, 3, and 7.

The situation is different when $W > r + r'n$. Specifically, the number of CMs used by the lightpaths coming from an IW (or heading for an OW) in this case is definitely less than W. Though an IW may also launch up to W 1-g lightpaths, the number of destinations of these W lightpaths is $r + r'n < W$. In other words, more than one lightpath may go to the same destination. Because the Rx at an output port can only receive one lightpath, multiple lightpaths must go to the same OW, rather than an output of a DM. According to the CM-sharing routing, the lightpaths from an IW to an OW should use the same CM. It follows that less than W CMs will be used by the lightpaths originating from an IW in the case of $W > r + r'n$.

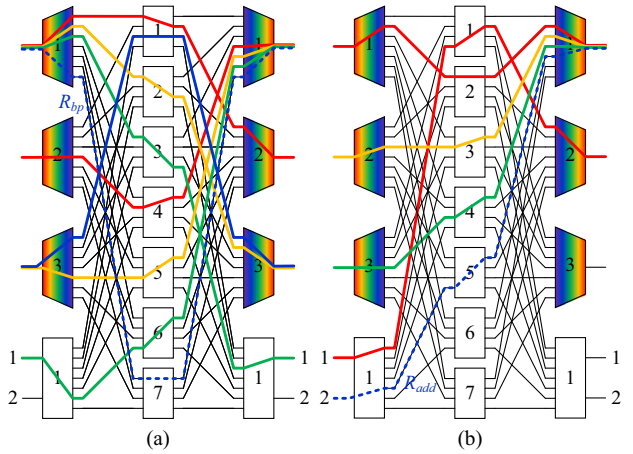

Fig. 5. Illustration of the worst case when $W \le r + r'n$, where $W = 4$, $r = 3$, $r' = 1$, and $n = 2$. (a) Request on the line side and (b) request on the A/D side.

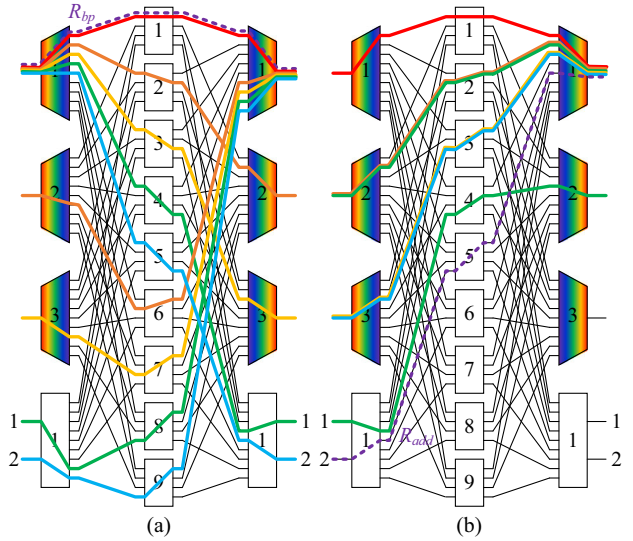

Fig. 6. Illustration of the worst case when $W > r + r'n$, where $W = 6$, $r = 3$, $r' = 1$, and $n = 2$. (a) Request on the line side and (b) request on the A/D side.

The same argument can apply to each OW in this case. An example is given by Fig. 6(a), where $W = 6$, $r = 3$, $r' = 1$, and $n = 2$. IW 1 can initiate up to $W = 6$ lightpaths. Since

$$W = 6 > r + r'n = 5,$$

at least two lightpaths will go to the same OW, e.g., the red and purple lightpaths from IW 1 to OW 1 in Fig. 6(a).

The discussion hints that the number of CMs needed to set up lightpaths may depend on the relationship of W and $r + r'n$.

Theorem 1: *under the CM-sharing routing strategy, the Clos-type OXC is WSNB on the line side and CDC on the A/D side, iff*

$$m \ge \begin{cases} \max\{n,\ W\} + W - 1 & \text{if } W \le r + r'n \\ 2\left(r + r'n\right) - 1 & \text{otherwise.} \end{cases}$$

Proof: see Appendix A. □

Figure 5 gives an example of the worst case that conforms to the CM-sharing strategy when $W \le r + r'n$ for a Clos-type OXC with $W = 4$, $r = 3$, $r' = 1$, and $n = 2$. In this example, we assume that all the lightpaths are 1-g lightpaths. Figure 5(a) is the worst case on the line side. The blue dashed line stands for a bypass request R_{bp} from IW 1 to OW 1. CMs 1, 2, and 3 are occupied by the lightpaths from IW 1 to OW 2, OW 3, and DM 1. Meanwhile, the lightpaths from IW 2, IW 3, and AM 1 to OW 1 employ CMs 4, 5, and 6. Thus, we need at least seven CMs to satisfy R_{bp}. Figure 5(b) plots the worst case for an add request R_{add} from AM 1 to OW 1. CM 1 is used by a lightpath from AM 1 to OW 2. CMs 2, 3, and 4 are occupied by lightpaths from IWs 1, 2, and 3 to OW 1. Hence, we need at least 5 CMs to satisfy R_{add}. In summary, it requires

$$m \ge \max\{7, 5\} = 7$$

CMs to make the Clos-type OXC WSNB on the line side and the CDC on the A/D side. This is consistent with the result of Theorem 1, i.e.,

$$m \ge \max\{n, W\} + W - 1 = \max\{2, 4\} + 4 - 1 = 7.$$

Figure 6 plots an example of the worst case when $W > r + r'n$ for the Clos-type OXC with $W = 6$, $r = 3$, $r' = 1$, and $n = 2$. Also, we assume that all the lightpaths are 1-g lightpaths. The worst case on the line side is depicted in Fig. 6(a), where the dashed line represents a bypass request R_{bp} from IW 1 to OW 1. The lightpaths from IW 1 to DM 1, OWs 1, 2, and 3 pass through CMs 4, 5, 1, 2, and 3, respectively. At the same time, the lightpaths from IW 2, IW 3, and AM 1 to OW 1 occupy CMs 6, 7, 8, and 9. R_{bp} can pass through the same CM with the lightpath from IW 1 to OW 1 because they have identical input and output. Thus, nine CMs are enough to set up a lightpath for R_{bp}. Figure 6(b) provides the worst case on the add side from AM 1 to OW 1. Five lightpaths from IWs 1, 2, and 3 to OW 1 traverse CMs 1, 2, and 3, respectively. At the same time, CM 4 is occupied by the lightpath, from AM 1 to OW 2. Among them, two lightpaths, both from IW 2 to OW 1, can share CM 2, and those from IW 3 to OW 1 can share CM 3. Thus, five CMs are enough to make up a lightpath for R_{add}. Combining the two cases, we thus need

$$m \ge \max\{9, 5\} = 9$$

CMs to construct a WSNB and CDC Clos-type OXC. This example verifies the correctness of Theorem 1, which states that

$$m \ge 2\left(r + r'n\right) - 1 = 2 \times (3 + 1 \times 2) - 1 = 9.$$

Remarks: *in a large-scale OXC, the number of fibers per link is large, while the number of wavelengths per fiber is relatively small, which corresponds to Case 1: $W < r + r'n$. If we set $n = W$, Theorem 1 actually indicates that the number of CMs m (i.e., the port count of WSSs) needed by a large-scale Clos-type OXC is $2W - 1$. That is, m is almost determined by W, instead of the number of fiber degrees of the OXC.*

In the near future, the channel spacing will be 300 GHz, and the entire C+L band will be utilized, which means the number of wavelengths per fiber will be 40. In this case, 1×79 WSSs will be needed according to Theorem 1. Clearly, this still poses a high requirement on the design of the WSS if the Clos-type OXC is deployed.

The Clos-type OXC can inherently support a PAYG model. In the early stage of network operation, we can deploy CMs with redundant ports. When expanding the capacity of the OXC, we only need to add some IWs, OWs, AMs, and DMs and connect them to the redundant ports of CMs. These newly added modules have the same dimension as that of the ones already installed in the system. Also, this upgrading procedure does not interrupt the existing lightpaths.

4. BUTTERFLY OXC ARCHITECTURES

This section proposes another design of the part in the dotted box to lower the requirement on the port count of WSSs (i.e., the number of CMs). The main idea is to expand one-stage OCSs on either side of the Clos-type OXC into two-stage OCSs, such that the number of CMs can be reduced. We first propose a structure called Butterfly OXC in Section 4.A, then present the routing constraints and a routing strategy for it in Section 4.B. We prove that it is WSNB on the line side and CDC on the A/D side in Section 4.C. We further perform transformations on the proposal to derive an expandable and more scalable OXC in Section 4.D.

A. Architecture

Figure 7 provides an overview of the Butterfly OXC, which is obtained from the Clos-type OXC by inserting m' $r' \times m$ OCSs, named central add OCS modules (CAMs) and numbered $1, \ldots, p, \ldots, m'$, between AMs and CMs, and m' $m \times r'$ OCSs, named central drop OCS modules (CDMs) and labeled $1, \ldots, q, \ldots, m'$, between CMs and DMs. Each CAM connects to each AM and each CM via one fiber, and each CDM connects to each DM and each CM via one fiber. As a result, each AM is an $n \times m'$ OCS, each CM is an $(r + m') \times (r + m')$ OCS, and each DM is an $m' \times n$ OCS.

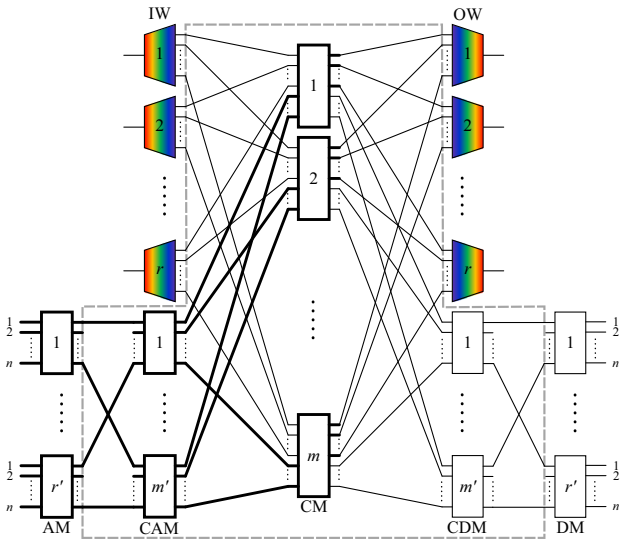

Fig. 7. Architecture of the Butterfly OXC, where the bolded part is C_{add}.

As the bolded part in Fig. 7 displays, r' AMs, m' CAMs, m CMs, and the last m' inputs and the first r outputs of m CMs form a classical Clos network, denoted by C_{add}. Similarly, r' DMs, m' CDMs, m CMs and the last m' outputs and the first r inputs of the CMs form a classical Clos network, denoted by C_{drop}.

At last, $r'n \le mr$ because the number of A/D ports should not be larger than that of the ports linked to the OWs/IWs.

B. Routing Constraints and λ-CM Binding Routing

Similar to the Clos-type OXC, there are two routing constraints in the Butterfly OXC as follows:

B1: the lightpaths from the same IW to different OWs/DMs cannot share the same CM;

B2: the lightpaths from different IWs/AMs to the same OW cannot share the same CM.

Since C_{add} and C_{drop} are two classical Clos networks, the Butterfly OXC has two additional routing constraints:

B3: the lightpaths from the same AM or to the same CM cannot share the same CAM;

B4: the lightpaths from the same CM or to the same DM cannot share the same CDM, which are the same as those of a Clos network.

To cope with constraints B1 and B2, we propose the routing strategy as follows.

λ-CM Binding Routing: CM w is only assigned to the request demanding the use of wavelength set $\mathbf{\Lambda}_w^{\omega}$.

This routing strategy precludes a lightpath from traversing CM w unless it employs wavelength w. Given that a wavelength can only be utilized by a single lightpath, this strategy eventually ensures that only one lightpath originating from an IW or heading to an OW can pass through a CM. In this way, the situations presented in B1 or B2 will never happen.

Constraints B3 and B4 can be addressed by the theory of Clos networks [19].

Lemma 1: *C_{add} and C_{drop} are SNB, iff* $m' \ge \min\{r + n - 1, r'n\}$.

C. Nonblocking and CDC Conditions

Combining Lemma 1 and the proposed λ-CM binding routing strategy, we can prove the following result.

Theorem 2: *under the λ-CM binding routing strategy, the Butterfly OXC is WSNB on the line side and CDC on the A/D side iff $m \ge W$ and* $m' \ge \min\{r + n - 1, r'n\}$.

Proof: see Appendix B. □

Consider a legal 2-g request $R_{\text{bp}}(1, 1, \mathbf{\Lambda}_1^2)$ in Fig. 8 as an example. As R_{bp} is legal, wavelengths 1 and 2 are idle on IW 1 and OW 1, and thus also available on the links from IW 1 to CM 1 and from CM 1 to OW 1. The λ-CM binding routing strategy ensures there is no lightpath that originates from IW 1 or heads for OW 1 passing through CM 1. It follows that CM 1 can be employed to set up a lightpath for R_{bp}. An example of an add request is $R_{\text{add}}(1, 1, 4, \mathbf{\Lambda}_2^2)$. The legality of R_{add} implies that wavelengths 2 and 3 are free on both OW 4 and the link from output 4 of CM 2 to OW 4. Similarly, the

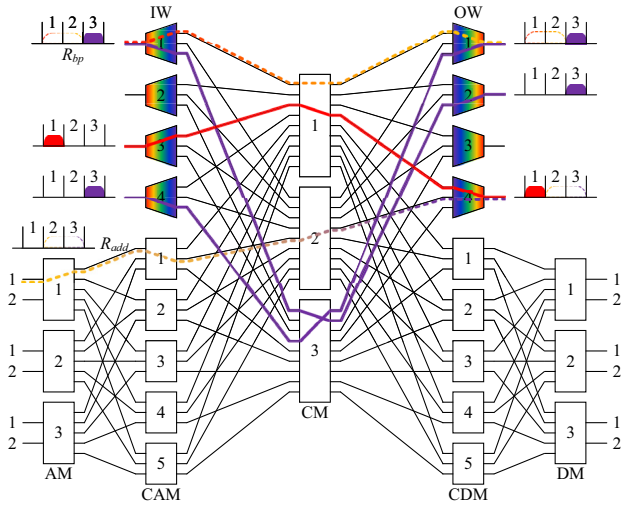

Fig. 8. Example of the Butterfly OXC, where $m = 3$, $W = 3$, $r = 4$, $r' = 3$, $m' = 5$, and $n = 2$.

λ-CM binding routing strategy guarantees that the CM 2 is available for R_{add}. Also, C_{add} can create a 2-g lightpath from input 1 of AM 1 to output 4 of CM 2. Hence, a 2-g lightpath from input 1 of AM 1 to OW 4 via CM 2 can be built for R_{add}.

The Butterfly OXC has the following two issues. First, though the number of CMs is reduced to W, the port count of each CM becomes $2r + n - 1$, as shown above. Second, it cannot achieve the PAYG property. All the OCSs in the OXC have to reserve some redundant ports at the start, to deal with future scale expansion. This implies a high initial installation cost, which violates the definition of PAYG property.

D. Derived Structure: Expandable Butterfly OXC

This part pursues a new design based on the Butterfly OXC, aiming to reduce the dimension of CMs while achieving the PAYG property. The size reduction of CMs is feasible since no lightpath will be established from C_{add} to C_{drop}, meaning that there is redundancy in each CM. Figure 9 details a CM. Recall that the first r input ports and output ports of CMs are respectively connected with r IWs and OWs, and the last $r + n - 1$ input ports and output ports are respectively connected with C_{add} and C_{drop}. Thus, each CM can be divided into four parts as follows:

(a) the red part between the first r input ports and output ports is served for the switch on the line side;
(b) the two green parts are used to perform remote lightpath dropping and local lightpath adding, respectively; and
(c) the yellow part connecting C_{add} and C_{drop} is wasted, since C_{add} never communicates with C_{drop}.

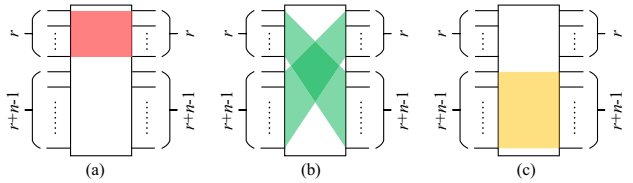

Fig. 9. Details of a CM: (a) area for the line side, (b) two areas for the A/D side, and (c) redundant area.

Suppose each CM is a $(2r+n-1)\times(2r+n-1)$ 3-D OCS, which is made up of $(r+r+n-1)^2$ mirrors. The redundancy of CMs can be precisely described by the expansion as follows:

$$(r+r+n-1)^2 = r^2 + 2r(r+n-1) + (r+n-1)^2,$$

which shows that a $(2r+n-1)\times(2r+n-1)$ OCS can be decomposed to a $r\times r$ OCS, two $r\times(r+n-1)$ OCSs, and a $(r+n-1)\times(r+n-1)$ OCS. Among them, the last one is the yellow part and can be removed.

After redundancy elimination, each CM can be replaced by three small OCSs as follows:

(a) $r\times r$ OCS, which is corresponding to the red part in Fig. 9(a), performs switching for bypass lightpaths, and thus is called bypass CM (bCM) and marked in red;
(b) $r\times(r+n-1)$ OCS, which corresponds to the green trapezoid from top left to bottom right in Fig. 9(b), performs switching for drop lightpaths, and thus is called drop CM (dCM) and marked in green;
(c) $(r+n-1)\times r$ OCS, which corresponds to the green trapezoid from bottom left to top right in Fig. 9(b), performs switching for add lightpaths, and thus is called add CM (aCM) and marked in green.

Additionally, each output of IW now needs a 1×2 space switch (SS). If there is a bypass request arrives at IW, the SS will connect the IW to an $r\times r$ bCM to set up a bypass lightpath; otherwise, it will link the IW to an $r\times(r+n-1)$ dCM to build a drop lightpath. Similarly, each input of an OW requires a 2×1 SS. At last, rearranging the position of every switching module, we can obtain a clear structure, as Fig. 10 displays. It is easy to see that the r' $n\times(r+n-1)$ AMs, $r+n-1$ $r'\times W$ CAMs, and W $(r+n-1)\times r$ aCMs form an SNB Clos network C_{add}, and the r' $(r+n-1)\times n$ DMs, $r+n-1$ $W\times r'$ CDMs, and W $r\times(r+n-1)$ dCMs form another SNB Clos network C_{drop}.

We have so far obtained a scalable OXC derived from the Butterfly OXC. However, it still does not support PAYG since

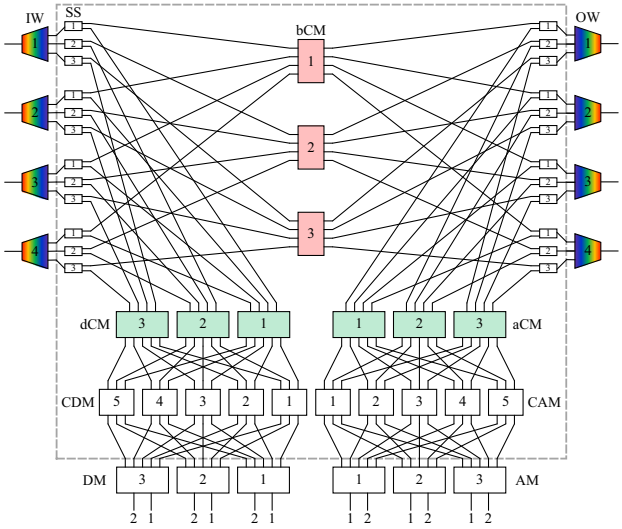

Fig. 10. OXC derived from the Butterfly OXC, where $W=3$, $r=4$, $r'=3$, $m'=5$, and $n=2$.

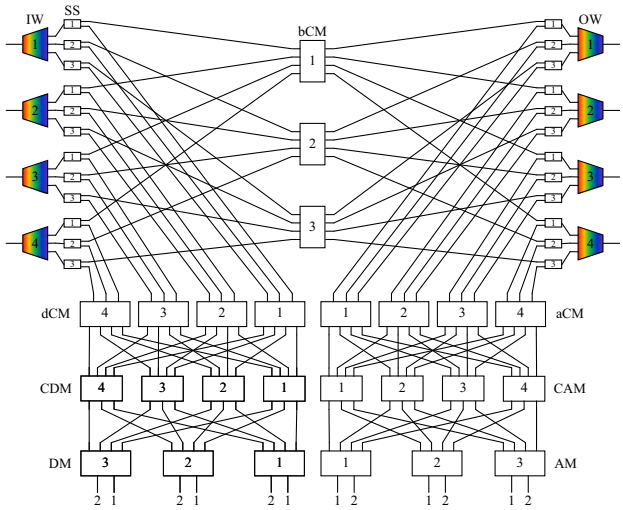

Fig. 11. Example of the expandable Butterfly OXC, where $W=3$, $r=4$, $r'=3$, $m'=4$, and $n=2$.

the port count of all the OCSs will increase with the expansion of the OXC.

We thus further modify this structure in two steps. In step 1, we connect each IW (OW) to only one dCM (aCM). In step 2, we install $n+W-1$ $r'\times r$ CDMs (CAMs) and r' $n\times(n+W-1)$ DMs (AMs) in C_{drop} and C_{add}, as Fig. 11 plots. After the modification, we obtain a new OXC structure called the expandable Butterfly OXC. It is obvious that the SNB feature of C_{drop} and C_{add} keeps unchanged after modification.

In the following, we first show that the expandable OXC is WSNB on the line side and CDC on the A/D side, and then explain that it can support a PAYG model.

We label the bCMs by $1,\ldots,b,\ldots,W$, from top to bottom, the aCMs by $1,\ldots,a,\ldots,r$, from left to right, and the dCMs by $1,\ldots,d,\ldots,r$, from right to left. On the add side, output a of CAM p is linked to input p of aCM a, and output β of aCM a is linked to input 2 of the 2×1 SS at input β of OW a. On the drop side, output 2 of the 1×2 SS at output d of IW α is linked to input d of dCM α, and output q of dCM d is linked to input d of CDM q.

In the expandable Butterfly OXC, the λ-CM binding routing strategy can be slightly modified as follows:

Revised λ-CM Binding Routing: bCM w is only assigned to the bypass request demanding the use of wavelength set $\mathbf{\Lambda}_w^{\omega}$.

Following the similar argument in Theorem 2, we can prove the following result:

Theorem 3: *under the revised λ-CM binding routing strategy, the expandable Butterfly OXC with* $m'\geq min\{W+n-1, r'n\}$ *is WSNB on the line side and CDC on the A/D side.*

Also, the expandable Butterfly OXC has the PAYG feature. At the beginning, only the CAM, CDM, and bCM have to reserve some redundant ports for future system expansion. When there is a need to increase the port count of the OXC, we only have to add some IWs, OWs, AMs, DMs, aCMs, and dCMs, the dimension of which is the same as that of the ones initially installed in the OXC, and connect them to the corresponding redundant ports of bCMs, CDMs, and CAMs.

5. APPLICATION AND COMPARISON

The three types of OXCs proposed in Sections 3 and 4 have their own strengths. In this section, we will first compare their scalability in port count and insertion loss, followed by a comparison with prior designs.

A. Comparison of Our Proposals

Compared to the Butterfly OXC and expandable Butterfly OXC, the Clos-type OXC has a lower insertion loss on the A/D side. The insertion loss of a typical WSS is 6 dB, and that of a typical OCS is 2 dB. Thus, the loss of the Clos-type OXC is 10 dB, that of the Butterfly OXC is 12 dB, and that of the expandable Butterfly OXC is 14 dB. Of course, both the Clos-type OXC and the Butterfly OXC have 14 dB insertion loss, while the expandable Butterfly OXC has a 18 dB insertion loss on the line side.

Because a bypass lightpath only needs to traverse a pair of WSSs on the line side, the filtering effect that it will suffer in all the OXCs proposed in this paper will be the same as that experienced in the standard OXC.

It is clear that, in terms of port count, the Butterfly OXC and expandable Butterfly OXC are more scalable than the Clos-type OXC because they only require $1 \times W$ WSSs, whereas the Clos-type OXC needs $1 \times (2W-1)$ WSSs. The 300 GHz transmission system will be commercial soon, meaning that the C+L band will contain 40 wavelengths. As Section 4 analyzes, the port count of WSSs needed in the expandable Butterfly OXC is 40. This means that, even based on current WSS products, the expandable Butterfly OXC is applicable. The Clos-type OXC will be feasible only if the port count of commercial WSSs can be further increased to 79 in the future. The reduction of the requirement for the dimension of WSSs by the Butterfly OXC and expandable Butterfly OXC is due to the use of a Clos network on the A/D side. This design coordinates with the λ-CM binding routing strategy very well, leading to the decline of the number of CMs from $2W-1$ to W. Additionally, the dimension of aCMs, bCMs, and dCMs in the expandable Butterfly OXC is smaller than that of CMs in the Butterfly OXC. In contrast, the λ-CM binding routing strategy cannot be applied to the Clos-type OXC. Consider the AMs and the CMs in Fig. 4, which constitute a two-stage Banyan network. Suppose CM w is assigned for the request demanding wavelength w. Two requests in an AM cannot be satisfied at the same time, if they both need to use wavelength w. That is, the Clos-type OXC is not CDC if the λ-CM binding routing strategy is applied.

The dimension of the OCS in the expandable Butterfly OXC is smaller than that in the Butterfly OXC, owing to the advantages gained from the redundancy elimination described in Section 4.D. That is, the expandable Butterfly OXC offers superior scalability in port count.

Our proposals improve the scalability with acceptable power consumption. Compared to the standard OXC, the Clos-type OXC and the expandable Butterfly OXC add some OCSs. According to [45,46], the power consumption per port of the OCS is ∼0.4 W. The Clos-type OXC and the expandable Butterfly OXC need $2W-1$ $N \times N$ OCSs and W $N \times N$ OCSs in addition on the line side, respectively, resulting in power consumptions that are $0.4N(2W-1)$ and $0.4NW$ units greater than the power consumption of the standard OXC.

B. Comparison with Other Proposals

Table 1 compares our designs with other OXC designs [10–13,15–18,20,24–37]. Table 1 only considers the line side, as most of the previous designs do not provide the design of the A/D system.

An $N \times N$ ring-type OXC in [30–34] is made up of k $N/k \times N/k$ small-scale standard OXCs. When $k=\sqrt{N}$, it requires $2N$ $1 \times \sqrt{N}$ WSSs. A lightpath traversing l small-scale OXCs will experience an insertion loss of $12l$ dB, where $l=1, 2, \ldots, \sqrt{N}$. The ring-type OXC is not a PAYG design because the port count of all the WSSs will increase with the expansion of the OXC.

HIER in [35–37] is obtained by replacing each $1 \times N$ WSS in a standard OXC with a $1 \times k$ WSS and k $1 \times m$ space switches, where $km=N$. To facilitate the comparison, we assume $k=m=\sqrt{N}$. It follows that it needs $2N$ $1 \times \sqrt{N}$ WSSs and $2N^{3/2}$ $1 \times \sqrt{N}$ OCSs. Each bypass lightpath goes through two space switches and two WSSs, thus suffering a loss

Table 1. Comparison of Different OXCs

		Cost to Support			WSS/AWG		OCS	
	Nonblocking	Flexible Grids	Insertion Loss	PAYG	Dimension	Number	Dimension	Number
Standard OXC	Yes	Low	12 dB	No	$1 \times N$	$2N$	–	–
Ring-type OXC [30–34]	No	Low	$12l$ dB $l=1, \ldots, \sqrt{N}$	No	$1 \times \sqrt{N}$	$2N$	–	–
HIER [10,35–37]	No	High	16 dB	No	$1 \times \sqrt{N}$	$2N$	$1 \times \sqrt{N}$	$2N^{3/2}$
OXC-Clos Network [15–18]	Yes	High	36 dB	Yes	$1 \times \sqrt{N}$	$8N-4\sqrt{N}$	–	–
Modular OXC [20]	Yes	Low	24 dB	Yes	$1 \times \sqrt{N}$	$2(N^{3/2}+N)$	–	–
HOXC [11,24–29]	No	Low	16 dB	No	$1 \times hN$	$2hN$	$(1+h)N \times (1+h)N$	1
AWG-based OXC [12,13]	Yes	–	14 dB	Yes	$1 \times W$	$2N$	$N \times N$	W
Clos-type OXC	Yes	Low	14 dB	Yes	$1 \times (2W-1)$	$2N$	$N \times N$	$2W-1$
Expandable Butterfly OXC	Yes	Low	18 dB	Yes	$1 \times W$	$2N$	$N \times N$	W

of 16 dB. HIER is not a PAYG design because the port count of all the OCSs and optical couplers in HIER increases with the expansion of the OXC.

As for the $N \times N$ OXC-Clos network in [15–18], it roughly needs $8N - 4\sqrt{N}$ $1 \times \sqrt{N}$ WSSs and $2N$ $1 \times (2\sqrt{N} - 1)$ WSSs to fulfill the SNB switching function if it does not support the flexible grids. As each lightpath has to traverse six WSSs, the loss is 36 dB. The OXC-Clos network inherits the merit of the Clos network, and thus can support a PAYG model.

The modular OXC proposed in [20] can be constructed from N $\sqrt{N} \times \sqrt{N}$ standard OXCs interconnected by $2N$ $1 \times \sqrt{N}$ WSSs. A lightpath goes through four WSSs, the loss of which is 24 dB. Similar to the OXC-Clos network, the modular OXC has the PAYG feature.

The HOXC reported in [11,24–29] consists of an OCS and a small-sized OXC. Let h be a decimal. It needs $2hN$ $1 \times hN$ WSSs and 1 $(1+h)N \times (1+h)N$ OCSs. A lightpath may need to pass through the OCS twice and the OXC once, and thus has an insertion loss of 16 dB if the OCS is a MEMS-based OCS. The HOXC lacks PAYG capability, since the OCS and the WSSs with high port count are needed at the initial stage to cope with future scale expansion.

The AWG-based OXC has ~ 14 dB insertion loss on the line side. Similar to our designs, it has the PAYG feature.

Table 1 confirms that our proposals meet all the properties P1 through P7 listed in Section 1. Different from the previous designs, the port count of WSSs in our proposals increases with W, rather than N, which matches the tendency toward more fibers per link and fewer wavelengths per fiber.

6. CONCLUSION

Optical networks in the near future call for large-scale, low-loss, and flex-grid OXCs. However, the scalability of standard OXCs is limited by the dimension of commercial WSSs. To address this issue, this paper proposes three hybrid OXCs, called Clos-type OXC, Butterfly OXC, and expandable Butterfly OXC, leveraging the complementary features of WSSs and OCSs. We show that our proposals have the following merits: (1) they are nonblocking on the line side and CDC on the A/D side, (2) the dimension of WSSs is solely determined by the number of wavelengths and does not increase with the number of fiber directions of the OXC, (3) they have low insertion loss and small filtering effect, and (4) they can support flexible grids. The Clos-type OXC is a superior option if the number of OCSs and the insertion loss on the A/D side are the major concerns, and the Butterfly OXC and expandable Butterfly OXC would be a better choice if the focus is primarily on the port count of WSSs.

APPENDIX A: PROOF OF THEOREM 1

It is trivial to show that the proposed OXC is colorless and directionless. Thus, we only need to prove that the OXC on the line side is WSNB and on the A/D side is contentionless.

Case 1: $W \le r + r'n$.

Consider a bypass request $R_{\text{bp}}(\alpha, \beta, \mathbf{\Lambda}_w^{\omega})$. R_{bp} may see the situation, where all other wavelengths are busy at IW α and OW β. In the worst case, each of the $W-\omega$ waveleng $W-\omega$ ths at IW α carries one 1-g lightpath, and these $W-\omega$ lightpaths will use up to $W-\omega$ CMs, as we explain at the beginning of this subsection. Similarly, the $W-\omega$ wavelengths at OW β will carry up to $W-\omega$ lightpaths, which can at most occupy $W-\omega$ CMs. Let $\boldsymbol{S}_\alpha$ and $\boldsymbol{S}_\beta$ be the sets of CMs used by the lightpaths originating from IW α and that heading for OW β, respectively. We have

$$|\boldsymbol{S}_\alpha| \le W - \omega$$

and

$$|\boldsymbol{S}_\beta| \le W - \omega.$$

It follows that the number of CMs unavailable for R_{bp} is

$$|\boldsymbol{S}_\alpha \cup \boldsymbol{S}_\beta| \le |\boldsymbol{S}_\alpha| + |\boldsymbol{S}_\beta| \le 2W - 2\omega,$$

where the inequality holds with equality when $\boldsymbol{S}_\alpha \cap \boldsymbol{S}_\beta = \phi$. R_{bp} can be satisfied only when there is at least one CM that is not occupied by the lightpaths that originate from IW α or go to OW β. We thus need

$$m \ge \max_{\omega \ge 1}\{2W - 2\omega + 1\} = 2W - 1 \qquad \textbf{(A.1)}$$

CMs to accommodate the request R_{bp}.

Consider an add request $R_{\text{add}}(\alpha', a, \beta, \mathbf{\Lambda}_w^{\omega})$. This request may see the situation, where all the other $n-1$ inputs of AM α' and all the other $W-\omega$ wavelengths on OW β are busy. In the worst case, $n-1$ lightpaths from AM α' use $n-1$ CMs and $W-\omega$ wavelengths on OW β carry 1-g lightpaths, which use $W-\omega$ CMs. Let $\boldsymbol{S}_{\alpha'}$ be the set of CMs occupied by the lightpaths from AM α'. We have

$$|\boldsymbol{S}_{\alpha'}| \le n - 1$$

and

$$|\boldsymbol{S}_\beta| \le W - \omega.$$

Therefore, the number of CMs unavailable for R_{add} is

$$|\boldsymbol{S}_{\alpha'} \cup \boldsymbol{S}_\beta| \le |\boldsymbol{S}_{\alpha'}| + |\boldsymbol{S}_\beta| = n + W - \omega - 1,$$

where the inequality holds with equality if $\boldsymbol{S}_{\alpha'} \cap \boldsymbol{S}_\beta = \phi$. We thus need

$$m \ge \max_{\omega \ge 1}\{n + W - \omega\} = n + W - 1 \qquad \textbf{(A.2)}$$

CMs to satisfy R_{add}. Since the A/D system is symmetrical, the contentionless condition for drop requests is the same as that for add requests.

Combining (A.1) and (A.2), we have the nonblocking condition on the line side and the CDC condition on the A/D side:

$$m \ge \max\{n, W\} + W - 1.$$

Case 2: $W > r + r'n$.

Considering a bypass request $R_{\text{bp}}(\alpha, \beta, \mathbf{\Lambda}_w^{\omega})$, which sees that all other $W-\omega$ wavelengths are busy at IW α and OW β. Both the $W-\omega$ busy wavelengths at IW α and those at OW β can carry up to $W-\omega$ 1-g lightpaths. Depending on the

relative magnitude of $W-\omega$ and $r+r'n-1$, there arise two subcases as follows:

Case 2.1: $W-\omega > r+r'n-1$.

In this case, $W-\omega$ 1-g lightpaths from IW α may visit $r-1$ OWs and $r'n$ outputs of all the r' DMs at most. Since $W-\omega > r+r'n-1$, at least two lightpaths from IW α will visit the same OW, as we show at the beginning of Section 3.B. Thus, $W-\omega$ 1-g lightpaths from IW α will use $r+r'n-1$ CMs in the worst case. Similarly, $W-\omega$ 1-g lightpaths directed toward IW β may utilize $r+r'n-1$ CMs in the worst case. We thus have

$$|\boldsymbol{S}_\alpha| \le r+r'n-1$$

and

$$|\boldsymbol{S}_\beta| \le r+r'n-1.$$

It follows that the number of CMs unavailable for R_{bp} is

$$|\boldsymbol{S}_\alpha \cup \boldsymbol{S}_\beta| \le |\boldsymbol{S}_\alpha| + |\boldsymbol{S}_\beta| \le 2\left(r+r'n\right)-2.$$

Therefore, we need

$$m \ge 2(r+r'n)-1 \tag{A.3}$$

CMs to set up a lightpath for R_{bp}.

Case 2.2: $W-\omega \le r+r'n-1$.

Both the $W-\omega$ lightpaths from IW α and those directed toward OW β will traverse $W-\omega$ CMs in the worst case. In other words

$$|\boldsymbol{S}_\alpha| \le W-\omega$$

and

$$|\boldsymbol{S}_\beta| \le W-\omega.$$

The number of CMs that cannot be used by R_{bp} is

$$|\boldsymbol{S}_\alpha \cup \boldsymbol{S}_\beta| \le |\boldsymbol{S}_\alpha| + |\boldsymbol{S}_\beta| = 2W-2\omega.$$

We thus need

$$m \ge \max_{\omega \ge 1}\{2W-2\omega\}+1 = 2\left(r+r'n\right)-1 \tag{A.4}$$

CMs to set up a lightpath for R_{bp}. Combining (A.3) and (A.4), we need

$$m \ge 2\left(r+r'n\right)-1 \tag{A.5}$$

CMs to accommodate the bypass request R_{bp}.

Following similar arguments, we need

$$m \ge r+r'n \tag{A.6}$$

CMs to set up a lightpath for an add request or a drop request.

(A.5) and (A.6) yield the following condition for Case 2:

$$m \ge 2\left(r+r'n\right)-1.$$

APPENDIX B: PROOF OF THEOREM 2

The λ-CM binding routing strategy implies the necessity. In the following, we show the sufficiency.

Consider a legal bypass request $R_{\text{bp}}(\alpha, \beta, \boldsymbol{\Lambda}_w^\omega)$. As R_{bp} is legal, all the wavelengths in $\boldsymbol{\Lambda}_w^\omega$ are unused on the input of IW α and the output of OW β. This implies the wavelengths in $\boldsymbol{\Lambda}_w^\omega$ on the link from IW α to CM w and those on the link from CM w to OW β must be free. The λ-CM binding routing strategy ensures that CM w has not been used by an existing lightpath originating from IW α or destined for OW β, making it available for establishing a lightpath for R_{bp}.

Consider a legal add request $R_{\text{add}}(\alpha', a, \beta, \boldsymbol{\Lambda}_w^\omega)$. Owing to the legality of R_{add}, the wavelengths in $\boldsymbol{\Lambda}_w^\omega$ are unused on OW β and on the link from output β of CM w to OW β. Also, the λ-CM binding routing strategy guarantees that CM w has not been used by an existing lightpath heading for OW β. According to Lemma 1, C_{add} can establish a ω-g lightpath from input a of AM α' to output β of CM w without rearranging the existing lightpaths in C_{add}. It follows that a new ω-g lightpath can be set up via CM w for R_{add}. As the OXC is symmetrical, a lightpath can always be established for a legal drop request without reconfiguration.

Since $1 \le w \le W$, the above argument indicates W CMs are enough to route all the bypass, add, and drop requests.

Funding. National Natural Science Foundation of China (62271306, 62331017); National Key Research and Development Program of China (2024YFB2908301).

Acknowledgment. Part of this work has been presented in IEEE CLEO-PR 2024.

REFERENCES

1. P. J. Winzer, "The future of communications is massively parallel," J. Opt. Commun. Netw. **15**, 783–787 (2023).
2. E. Park, "Looking ahead to 1600G" (Acacia, 2024), https://acacia-inc.com/blog/looking-ahead-to-1600g/.
3. J. Ozaki, Y. Ogiso, H. Yamazaki, *et al.*, "C+L-band InP-based coherent driver modulator enabled net-1.8 Tbps/λ transmission," J. Lightwave Technol. **43**, 1972–1978 (2025).
4. H. Li, D. Wang, and B. Ye, "Optical cross-connect technology and application" (ZTE, 2022), https://www.zte.com.cn/global/about/magazine/zte-technologies/2022/6-en/special-topic–intelligent-e-otn/5.html.
5. HUAWEI, "OSN 9800 P32," https://carrier.huawei.com/~/media/cnbgv2/download/products/networks/wdm-otn/osn-9800-p32-en.pdf.
6. ZTE, "ZXONE 9700," https://www.zte.com.cn/global/product_index/optical-network-en/item01-en/zxine-9700-en/zxine-9700-en.html.
7. NEC, "DW7000," https://id.nec.com/en_ID/PDF/Telco-Optic/IP-Backbone/DW7000_Brochure.pdf.
8. Y. Ma, L. Stewart, J. Armstrong, *et al.*, "Recent progress of wavelength selective switch," J. Lightwave Technol. **39**, 896–903 (2021).
9. Finisar, "Finisar Australia releases the world's first flexgrid twin 1x48 wavelength selective switch," Oct. 2021, https://www.globenewswire.com/news-release/2021/10/04/2307857/0/en/Finisar-Australia-Releases-the-World-s-First-Flexgrid-Twin-1x48-Wavelength-Selective-Switch.html.
10. T. Ban, H. Hasegawa, K. Sato, *et al.*, "A novel large-scale OXC architecture and an experimental system that utilizes wavelength path switching and fiber selection," Opt. Express **21**, 469–477 (2013).
11. M. Jinno, "Spatial channel cross-connect architectures for spatial channel networks," IEEE J. Sel. Top. Quantum Electron. **26**, 3600116 (2020).
12. C.-K. Chan, E. Kong, F. Tong, *et al.*, "A novel optical-path supervisory scheme for optical cross connects in all-optical transport networks," IEEE Photonics Technol. Lett. **10**, 899–901 (1998).

13. K. A. McGreer, "Arrayed waveguide gratings for wavelength routing," IEEE Commun. Mag. **36**(12), 62–68 (2002).
14. Coherent, "Optical circuit switch," https://www.coherent.com/networking/optical-circuit-switch.
15. J. Lin, T. Chang, Z. Zhai, *et al.*, "Wavelength selective switch-based Clos network: blocking theory and performance analyses," J. Lightwave Technol. **40**, 5842–5853 (2022).
16. K. Chen, T. Ye, H. He, *et al.*, "Modular optical cross-connects (OXCs) for large-scale optical networks," IEEE Photon. Technol. Lett. **31**, 763–766 (2019).
17. H. Mehrvar, S. Li, and E. Bernier, "Dimensioning networks of ROADM cluster nodes," J. Opt. Commun. Netw. **15**, C166–C178 (2023).
18. Y. Yao, T. Ye, and N. Deng, "Wide-sense nonblocking conditions for flex-grid OXC-Clos networks," IEEE J. Sel. Areas Commun. **43**, 1809–1822 (2025).
19. S. C. Liew and T. T. Lee, *Principles of Broadband Switching and Networking* (Wiley, 2010).
20. Z. Cheng, T. Ye, Y. Zhu, *et al.*, "A three-phase modularization approach of OXC for large-scale ROADM," J. Lightwave Technol. **41**, 7318–7327 (2023).
21. G. Danilewicz, W. Kabaciński, and R. Rajewski, "Strict-sense non-blocking space-wavelength-space switching fabrics for elastic optical network nodes," J. Opt. Commun. Netw. **8**, 745–756 (2016).
22. W. Kabaciński, M. Michalski, and M. Abdulsahib, "The strict-sense nonblocking elastic optical switch," in *International Conference on High Performance Switching and Routing* (IEEE, 2015).
23. W. Kabaciński, M. Michalski, and R. Rajewski, "Strict-sense non-blocking WSW node architectures for elastic optical networks," J. Lightwave Technol. **34**, 3155–3162 (2016).
24. K.-I. Sato and H. Hasegawa, "Optical networking technologies that will create future bandwidth-abundant networks," J. Opt. Commun. Netw. **1**, A81–A93 (2009).
25. K. Ishii, S. Mitsui, H. Hasegawa, *et al.*, "Development of hierarchical optical path cross-connect systems employing wavelength/waveband selective switches," J. Opt. Commun. Netw. **3**, 559–567 (2011).
26. M. Jinno, T. Kodama, and T. Ishikawa, "Feasibility demonstration of spatial channel networking using SDM/WDM hierarchical approach for peta-b/s optical transport," J. Lightwave Technol. **38**, 2577–2586 (2020).
27. K. Nakada, H. Takeshita, Y. Kuno, *et al.*, "Single multicore-fiber bidirectional spatial channel network based on spatial cross-connect and multicore EDFA efficiently accommodating asymmetric traffic," in *Optical Fiber Communication Conference* (Optica Publishing Group, 2023), paper M4G.7.
28. H. Yuasa, K. Cruzado, Y. Mori, *et al.*, "Multi-layered optical network architecture with coarse-granularity-routing optical bypass," in *International Conference on Optical Network Design and Modeling* (IEEE, 2024).
29. K. Anazawa, T. Mano, T. Inoue, *et al.*, "Reconfigurable transport networks to accommodate much more traffic demand," in *International Conference on Information Networking* (IEEE, 2021), pp. 361–366.
30. Y. Iwai, H. Hasegawa, and K.-I. Sato, "OXC hardware scale reduction attained by using interconnected subsystem architecture," in *Optical Fiber Communication Conference/National Fiber Optic Engineers Conference* (Optica Publishing Group, 2013), paper NW1J.2.
31. H. Ishida, H. Hasegawa, and K.-I. Sato, "Hardware scale and performance evaluation of a compact subsystem modular optical cross connect that adopts tailored add/drop architecture," J. Opt. Commun. Netw. **7**, 586–596 (2015).
32. Y. Iwai, H. Hasegawa, and K.-I. Sato, "A large-scale photonic node architecture that utilizes interconnected OXC subsystems," Opt. Express **21**, 478–487 (2013).
33. Y. Tanaka, H. Hasegawa, and K.-I. Sato, "Performance analysis of large-scale OXC that enables dynamic modular growth," Opt. Express **23**, 5994–6006 (2015).
34. M. Niwa, Y. Mori, H. Hasegawa, *et al.*, "Tipping point for the future scalable OXC: what size M × M WSS is needed?" J. Opt. Commun. Netw. **9**, A18–A25 (2017).
35. T. Ban, H. Hasegawa, K. Sato, *et al.*, "A novel large-scale OXC architecture that employs wavelength path switching and fiber selection," in *European Conference and Exhibition on Optical Communication* (IEEE, 2012).
36. H.-C. Le, H. Hasegawa, and K.-I. Sato, "Performance evaluation of large-scale OXCs that employ multi-stage hetero-granular optical path switching," in *European Conference and Exhibition on Optical Communication* (IEEE, 2013).
37. H.-C. Le, H. Hasegawa, and K.-I. Sato, "Performance evaluation of large-scale multi-stage hetero-granular optical cross-connects," Opt. Express **22**, 3157–3168 (2014).
38. J. Pedro and S. Pato, "On scaling transport networks for very high nodal degree ROADM nodes using state-of-the-art optical switch technology," in *International Conference on Transparent Optical Networks* (IEEE, 2015).
39. K. Sato, Y. Mori, H. Hasegawa, *et al.*, "Algorithm for raising OXC port count to meet traffic growth at minimum cost," J. Opt. Commun. Netw. **9**, A263–A270 (2017).
40. T. Matsuo, R. Shiraki, Y. Mori, *et al.*, "Architecture and performance evaluation of fiber-granularity routing networks with supplemental grooming by wavelength conversion," J. Opt. Commun. Netw. **15**, 541–552 (2023).
41. Z. Huang, S. Yang, Z. Zheng, *et al.*, "Highly compact twin 1 × 35 wavelength selective switch," J. Lightwave Technol. **41**, 233–239 (2023).
42. Calient.AI, "S320," https://www.calient.net/.
43. Polatis, "Polatis 576," https://www.polatis.com/polatis576.asp.
44. HUAWEI, "Full series of 400 G/800G," 2024, https://carrier.huawei.com/~/media/cnbgv2/download/products/network-energy/Full-Series-of-400G-800G-Solution-en.pdf.
45. "Polatis Series 6000i," https://www.viavisolutions.com/en-us/literature/polatis-series-6000-osm-network-switch-module-data-sheets-en.pdf.
46. "Polatis Series 7000i," https://www.sevensix.co.jp/wp-content/uploads/Polatis_7000i_Data_Sheet.pdf.